Velocity Feedback Control of Swing Phase for 2-DoF Robotic Leg Driven by Electro-hydraulic Servo System

Jian Zhang, Lie Yu and Lei Ding

***Abstract*—This paper presents a computational model for a nonlinear two degree-of-freedom (2-DoF) robotic leg. The model is based on a mathematical model of two connected body segments to mimic the lower thigh and shank of human leg. Two sets of electro-hydraulic servo systems (EHSS) are seperately used to drive the robotic thigh and shank. The dynamic of EHSS is accurately developed to exhibit the relationship of the input current and the actuated force\torque. A velocity observer is used to estimate the angular velocities of the robotic thigh and shank. Then, a velocity feedback controller is proposed to track the hip and knee joints movements of robotic leg. The simulation results show that the velocity feedback controller gives better tracking performances in term of position control strategy when compared with the conventional PID controller.**

***Index Terms*—Robotic leg, Electro-hydraulic servo systems, Velocity feedback controller, PID controller.**

I. Introduction

The drive mechanism with a two degree-of-freedom (2-DoF) driver has been widely used as mechanical tools in the industry manufactures, including robotic systems, injection machines and boring machines [1]–[3]. Generally, the actuation for a 2-DoF driver is selected to be motors or electrohydraulic servo systems (EHSS). Many researches and applications of motor have been made to control the 2-DoF driver [4]–[6]. However, in this paper, the realization of 2-DoF driving technologies is achieved by utilizing two sets of EHSS for their ability of high load efficiency, fast response, and high tracking accuracy [7].

The modeling of EHSS is extremely difficult for some nonlinear time-varying phenomena, such as the relationship between input current and output flow, fluid compressibility, deadband due to the internal leakage and external load [8]. In addition, the values of hydraulic parameters may vary due to temperature changes and air entrapment in the hydraulic fluid. Based on the desired objectives, control strategies for EHSS can be classified as position control [9]–[12], velocity control [13] and force/torque control [14]–[15]. For any one of the control strategies, the controller designs will directly affect the tracking performances of EHSS. Generally, the PID controller is most widely used due to its simple control structure, ease of design and low cost [16]. However, the PID controller is completely independent of the mathematical model of EHSS.

In this paper, a 2-DoF robotic leg is introduced which is driven by EHSS for both the robotic thigh and shank. The modeling for robotic leg and EHSS is built based on the transformation of Lagrange equation and fluid equation. Additionally, the velocity is estimated using an observer and the velocity feedback controller is proposed though the actual position and estimated velocities. The simulation results show that the proposed velocity feedback controller provides less tracking lag and less mean absolute error (MAE) than the conventional PID controller.

II. Method

In this section, the dynamic models are separately derived for the EHSS and 2-DoF robotic leg. This analysis primarily builds the nonlinear model of the EHSS dynamics, and shows the process of the actuator driving the robotic leg. Similar approaches to modeling of EHSS have been reported in [17]–[18].

The 2-DoF robotic leg under consideration is drafted in Fig. 1. The robotic leg consists of two parts including thigh and shank. Two sets of EHSS are placed to drive the robotic thigh and shank.

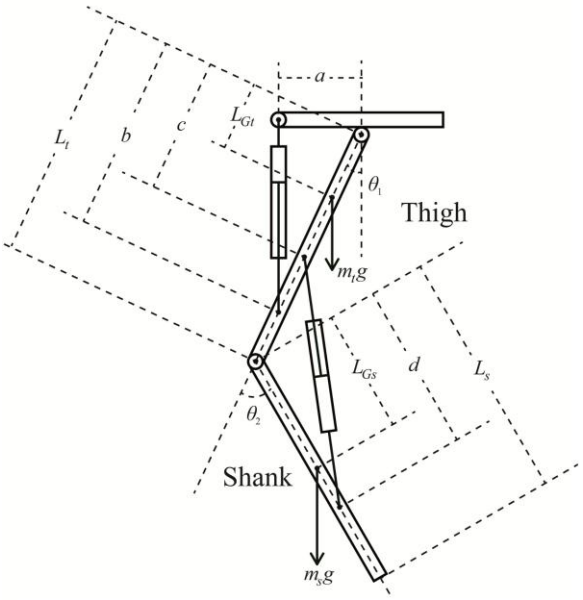

Fig. 1. Schematic Diagram of the EHSS and 2-DoF robotic leg

Manuscript received February 18th, 2016. This work was supported by the National Natural Science Foundation of China under Grant No. 41374148 and Educational Commission of Hubei Province of China under Grant No. Q20111306.

Jian Zhang is now with College of Computer Science, Yangtze University, JingZhou, China. (e-mail: zhangjian0716@126.com).

Lie Yu is with the School of Electronic and Electrical Engineering, Wuhan Textile University, Wuhan, China. (Corresponding author to provide phone: +86 18607155647; e-mail: honyeal@whut.edu.cn).

Lei Ding is with the School of Information and Engineering, Wuhan University of Technology, WuHan, China. (e-mail: 398487325@qq.com).

A. Modeling of Robotic Leg

The dynamic of 2-DoF robotic leg can be constructed by Lagrange equation as follows:

$$H(q)\ddot{q}+C(q,\dot{q})\dot{q}+G(q)=T \tag{1}$$

In [19], the $\ddot{\theta}_1$ and $\ddot{\theta}_2$ are derived and developed based on the double segment compound pendulums and Lagrange equation. However, the derived formula of $\ddot{\theta}_1$ includes the expression of $\ddot{\theta}_2$, and the derived formula of $\ddot{\theta}_2$ includes the expression of $\ddot{\theta}_1$. The coupling of $\ddot{\theta}_1$ and $\ddot{\theta}_2$ can not be neglected. Based on this, we use the transformation of Lagrange equation to eliminate the interrelationship between $\ddot{\theta}_1$ and $\ddot{\theta}_2$.

$$\ddot{q}=H^{-1}(q)(T-C(q,\dot{q})\dot{q}-G(q)) \tag{2}$$

where

$$H^{-1}=\begin{bmatrix}H_{11} & H_{12}\\ H_{21} & H_{22}\end{bmatrix}\quad C=\begin{bmatrix}C_{11} & C_{12}\\ C_{21} & C_{22}\end{bmatrix}\quad G=\begin{bmatrix}G_1\\ G_2\end{bmatrix}$$
$$q=\begin{bmatrix}\theta_1\\ \theta_2\end{bmatrix}\quad T=\begin{bmatrix}T_t\\ T_s\end{bmatrix} \tag{3}$$

where H, C and G are the inertia matrix, Coriolis matrix and gravity vector, respectively, T_t and T_s are the torques actuated severally on lower thigh and shank. θ_1 and θ_2 are the rotary angles of thigh and shank as shown in Fig. 1.

The elements of matrix H^{-1}, C and G can be expressed as follows:

$$H_{11}=\frac{4(\mathrm{m_sL_s^2}+4\mathrm{I_s})}{H_{note}}$$
$$H_{12}=\frac{-4(4\mathrm{I_s}+2\mathrm{m_sL_tL_s}\cos(\theta_2)+\mathrm{m_sL_s^2})}{H_{note}}$$
$$H_{21}=\frac{-4(4\mathrm{I_s}+2\mathrm{m_sL_tL_s}\cos(\theta_2)+\mathrm{m_sL_s^2})}{H_{note}}$$
$$H_{22}=\frac{4(4\mathrm{I_t}+4\mathrm{m_sL_t^2}+4\mathrm{m_sL_tL_s}\cos(\theta_2)+\mathrm{m_sL_s^2}+\mathrm{m_tL_t^2}+4\mathrm{I_s})}{H_{note}}$$
$$H_{note}=4\mathrm{I_tm_sL_s^2}+16\mathrm{I_tI_s}+4\mathrm{m_s^2L_t^2L_s^2}+16\mathrm{m_sL_t^2I_s}+\mathrm{m_tL_t^2m_sL_s^2}+4\mathrm{m_tL_t^2I_s}-4\mathrm{m_s^2L_t^2L_s^2}(\cos(\theta_2))^2$$

$$C_{11}=-\mathrm{L_tm_s}(-\cos(\theta_1+\theta_2)\sin(\theta_2)+\sin(\theta_1+\theta_2)\cos(\theta_2))\mathrm{L_{Gs}}\dot{\theta}_1$$
$$C_{12}=-2\mathrm{L_tm_s}(-\cos(\theta_1+\theta_2)\sin(\theta_2)+\sin(\theta_1+\theta_2)\cos(\theta_2))\mathrm{L_{Gs}}\dot{\theta}_2$$
$$C_{21}=0$$
$$C_{22}=\mathrm{L_tm_s}(-\cos(\theta_1+\theta_2)\sin(\theta_2)+\sin(\theta_1+\theta_2)\cos(\theta_2))\mathrm{L_{Gs}}\dot{\theta}_2$$
$$G_1=\mathrm{m_tgL_{Gt}}\sin(\theta_1)-\mathrm{m_sg}(-\mathrm{L_t}\sin(\theta_2)-\mathrm{L_{Gs}}\sin(\theta_1+\theta_2))$$
$$G_2=\mathrm{m_sgL_{Gs}}\sin(\theta_1+\theta_2) \tag{4}$$

where m_t is the thigh mass, m_s is the shank mass, L_t is the thigh length, L_s is the shank length, L_{Gt} is the the position of the center of the thigh mass, L_{Gs} is the the position of the center of the shank mass, I_t is the thigh inertia and I_s is the shank inertia.

The $\ddot{\theta}_1$ and $\ddot{\theta}_2$ can be obtained using the transformation of Lagrange equation in Eq. (2). However, the expressions in Eq. (4) give that the θ_1, θ_2, $\dot{\theta}_1$ and $\dot{\theta}_2$ should also be acquired. For simulation, the θ_1, θ_2, $\dot{\theta}_1$ and $\dot{\theta}_2$ can be written as:

$$\begin{cases}\dot{\theta}_1(t+1)=\dot{\theta}_1(t)+\ddot{\theta}_1(t)dt\\ \dot{\theta}_2(t+1)=\dot{\theta}_2(t)+\ddot{\theta}_2(t)dt\\ \theta_1(t+1)=\theta_1(t)+\dot{\theta}_1(t)dt+0.5\ddot{\theta}_1(t)dtdt\\ \theta_2(t+1)=\theta_2(t)+\dot{\theta}_2(t)dt+0.5\ddot{\theta}_2(t)dtdt\end{cases} \tag{5}$$

B. Modeling of Electro-Hydraulic Servo Systems

As shown in Fig. 1, two sets of EHSS generate the force\torque to drive the robotic thigh and shank. For the EHSS, the driving torque T can be calculated as:

$$T=FH \tag{6}$$

where

$$T=\begin{bmatrix}T_t\\ T_s\end{bmatrix}$$
$$F=\begin{bmatrix}F_t & 0\\ 0 & F_s\end{bmatrix}=\begin{bmatrix}P_{1t}A_{p1}-P_{2t}A_{p2} & 0\\ 0 & P_{1s}A_{p1}-P_{2s}A_{p2}\end{bmatrix}$$
$$H=\begin{bmatrix}H_t\\ H_s\end{bmatrix} \tag{7}$$

where F_t is the driving force for the robotic thigh joint, F_s is the driving force for the robotic shank joint, P_{1t} and P_{1s} are the head-side pressure of hydraulic for the robotic thigh and shank, respectively; P_{2t} and P_{2s} are the rod-side pressure of hydraulic for the robotic thigh and shank, respectively; A_{p1} is the head-side area; A_{P2} is the rod-side area; H_t and H_s are the arm of force for the robotic thigh and shank, respectively. Due to the geometry of the robot system, the H_t and H_s can be computed as:

$$\begin{cases}H_t=\dfrac{ab\sin(\theta_1)}{\sqrt{a^2+b^2-2ab\sin(\theta_1)}}\\ H_s=\dfrac{-(L_t-c)d\cos(\theta_2)}{\sqrt{(L_t-c)^2+d^2+2(L_t-c)d\cos(\theta_2)}}\end{cases} \tag{8}$$

where a, b, c and d are the geometry lengths of the robotic thigh and shank as shown in Fig. 1.

In Eq. (7), the A_{p1} and A_{P2} can be calculated through the following formulas when the bore diameter D_1 and the rod diameter D_2 are acquired.

$$\begin{cases}A_{p1}=\dfrac{\pi D_1^2}{4}\\ A_{p2}=\dfrac{\pi(D_1^2-D_2^2)}{4}\end{cases} \tag{9}$$

As the the rod diameter D_2 is even less than the bore diameter D_1, the Eq. (5) can be simplified as

$$A_{p2}=\frac{\pi(D_1^2-D_2^2)}{4}\approx\frac{\pi D_1^2}{4}=A_{p1} \tag{10}$$

Substituting the Eq. (10) into Eq. (7) , the actuated force can be simplified as

$$F=\begin{bmatrix}F_t & 0\\ 0 & F_s\end{bmatrix}=\begin{bmatrix}(P_{1t}-P_{2t})A_{p1} & 0\\ 0 & (P_{1s}-P_{1s})A_{p1}\end{bmatrix} \tag{11}$$

Neglecting the external leakage, the pressure dynamics in actuator chambers can be described as

$$\begin{cases} \dot{P}_{1t} = \dfrac{\beta}{V_{1t}}(-A_{p1}v_{pt} - C_t P_{Lt} + Q_{1t}) \\ \dot{P}_{2t} = \dfrac{\beta}{V_{2t}}(A_{p1}v_{pt} + C_t P_{Lt} - Q_{2t}) \\ \dot{P}_{1s} = \dfrac{\beta}{V_{1s}}(-A_{p1}v_{ps} - C_t P_{Ls} + Q_{1s}) \\ \dot{P}_{2s} = \dfrac{\beta}{V_{2s}}(A_{p1}v_{ps} + C_t P_{Ls} - Q_{2s}) \end{cases} \tag{12}$$

where $V_{1t}=V_0+A_{p1}x_{pt}$, $V_{2t}=V_0-A_{p1}x_{pt}$, $V_{1s}=V_0+A_{p1}x_{ps}$, $V_{2s}=V_0-A_{p1}x_{ps}$ are the control volumes of the actuator chambers, V_0 is chamber volume such that at $x_{pt}=0$, $V_{1t}=V_{2t}=V_0$ or $x_{ps}=0$, $V_{1s}=V_{2s}=V_0$; β is the effective bulk modulus in the chambers; x_{pt} and x_{ps} are the load velocity of the robotic thigh and shank, respectively; $P_{Lt}=P_{1t}-P_{2t}$ and $P_{Ls}=P_{1s}-P_{2s}$ are the load pressure of the dynamic actuator of the robotic thigh and shank, respectively; C_t is the coefficient of the total internal leakage of the actuator due to the pressure; Q_{1t} *and* Q_{1s} are the supplied flow rate to the forward chamber, and Q_{2t} *and* Q_{2s} are the return flow rate of the return chamber. Q_{1t}, $Q_{2t,}$ Q_{1s} and Q_{2s} are related to the spool valve displacement of the servo-valve x_v.

$$\begin{cases} Q_{1t} = k_q x_{vt}[s(x_{vt})\sqrt{P_s - P_{1t}} + s(-x_{vt})\sqrt{P_{1t} - P_r}] \\ Q_{2t} = k_q x_{vt}[s(x_{vt})\sqrt{P_2 - P_r} + s(-x_{vt})\sqrt{P_s - P_{1t}}] \\ Q_{1s} = k_q x_{vs}[s(x_{vs})\sqrt{P_s - P_{1s}} + s(-x_{vs})\sqrt{P_{1s} - P_r}] \\ Q_{2s} = k_q x_{vs}[s(x_{vs})\sqrt{P_2 - P_r} + s(-x_{vs})\sqrt{P_s - P_{1s}}] \end{cases} \tag{13}$$

where

$$k_q = C_d w\sqrt{\frac{2}{\rho}} \tag{14}$$

$s(x)$ is defined as

$$s(x) = \begin{cases} 1 & if\ x \geq 0 \\ 0 & if\ x < 0 \end{cases} \tag{15}$$

where k_q is the valve discharge gain, C_d is the discharge coefficient, w is the spool valve area gradient, ρ is the density of hydraulic oil, P_s is the supply pressure of the fluid, and P_r is the return pressure.

However, the x_{pt}, v_{pt}, x_{ps} and v_{ps} can be calculated as

$$\begin{cases} x_{pt} = \sqrt{a^2 + b^2 - 2ab\sin(\theta_1)} - L_0 - x_{p0} \\ v_{pt} = \dfrac{-2ab\dot{\theta}_1\cos(\theta_1)}{\sqrt{a^2 + b^2 - 2ab\sin(\theta_1)}} \\ x_{ps} = \sqrt{(L_t - c)^2 + d^2 + 2(L_t - c)d\cos(\theta_2)} - L_0 - x_{p0} \\ v_{ps} = \dfrac{-2(L_t - c)d\sin(\theta_2)}{\sqrt{(L_t - c)^2 + d^2 + 2(L_t - c)d\cos(\theta_2)}} \end{cases} \tag{16}$$

where L_0 is the cylinder dead length and x_{p0} is the piston position when the volumes are equal on both cylinder sides.

Since a high-response servo valve is used, it is assumed that the current applied to the servo valve is directly proportional to the spool position, then the following equation is given by $x_v=k_c i$, where k_c is a positive electrical constant, and i is the input current. Thus, from Eq. (11), $s(x_v)=s(i)$. Then Eq. (13) can be rewritten as

$$\begin{cases} Q_{1t} = g_s R_{1t} i_t \\ Q_{2t} = g_s R_{2t} i_t \\ Q_{1s} = g_s R_{1s} i_s \\ Q_{2s} = g_s R_{2s} i_s \end{cases} \tag{17}$$

where $g_s=k_q k_c$ and

$$\begin{cases} R_{1t} = s(i_t)\sqrt{P_s - P_{1t}} + s(-i_t)\sqrt{P_{1t} - P_r} \\ R_{2t} = s(i_t)\sqrt{P_{2t} - P_r} + s(-i_t)\sqrt{P_s - P_{2t}} \\ R_{1s} = s(i_s)\sqrt{P_s - P_{1s}} + s(-i_s)\sqrt{P_{1s} - P_r} \\ R_{2s} = s(i_s)\sqrt{P_{2s} - P_r} + s(-i_s)\sqrt{P_s - P_{2s}} \end{cases} \tag{18}$$

Based on the Eq. (12) and (18), we have

$$\begin{cases} \dot{P}_{Lt} = \dot{P}_{1t} - \dot{P}_{2t} = (\dfrac{R_{1t}}{V_{1t}} + \dfrac{R_{2t}}{V_{2t}})\beta g_s i_t - (\dfrac{1}{V_{1t}} + \dfrac{1}{V_{2t}})(\beta C_t P_{Lt} + A_{p1}v_{pt}) \\ \dot{P}_{Ls} = \dot{P}_{1s} - \dot{P}_{2s} = (\dfrac{R_{1s}}{V_{1s}} + \dfrac{R_{2s}}{V_{2s}})\beta g_s i_s - (\dfrac{1}{V_{1s}} + \dfrac{1}{V_{2s}})(\beta C_t P_{Ls} + A_{p1}v_{ps}) \end{cases} \tag{19}$$

Therefore, the derivation of the actuated force F_t and F_s can be obtained by

$$\dot{F} = \begin{bmatrix} \dot{F}_t & 0 \\ 0 & \dot{F}_s \end{bmatrix} = \begin{bmatrix} \dot{P}_{Lt}A_{p1} & 0 \\ 0 & \dot{P}_{Ls}A_{p1} \end{bmatrix} \tag{20}$$

In practical working conditions, the P_{1t}, P_{2t}, P_{1s} and P_{2s} are all bounded by P_s and P_r, i.e. $0<P_r<P_{1t}<P_s$, $0<P_r<P_{2t}<P_s$, $0<P_r<P_{1s}<P_s$ and $0<P_r<P_{2s}<P_s$. In simulation process, the P_{Lt} and P_{Ls} are both bounded by P_s, i.e. $-P_s< P_{Lt} < P_s$ and $-P_s< P_{Ls} < P_s$.

III. CONTROLLER DESIGN

The aim of the controller is to evaluate the tracking performance of EHSS such that the desired and actual positions should be obtained before controller design. In this paper, the desired positions θ_{1d} and θ_{2d} are designed to be the rotary angles of human hip and knee joints in one gait cycle. Then, the controller design can be made at a sampling frequency of fs=1000Hz to examine the behavior of the system.

A. Design of the PID Controller

To test the position tracking performance of 2-DoF robotic leg driven by EHSS, a feedback controller is added into this system where the actual positions (i.e., θ_1 and θ_2) of thigh and shank are then compared with the desired positions defined in Eq. (21). The error between the desired position and actual position is calculated and fed back to the system. The required torques to compensate these errors are generated by the input currents into the servo valves, which are figured out by a Proportional-Integral-Derivative (PID) controller for both lower thigh and shank as shown in Eq. (22). Fig. 2 illustrates the block diagram for the conventional PID controller that is added to the nonlinear 2-DoF robotic leg system. The conventional PID controller can be constructed as follows.

$$i(t) = K_p e(t) + K_i \int e(t)dt + K_d \frac{de(t)}{dt} \tag{21}$$

where

$$i=\begin{bmatrix} i_t \\ i_s \end{bmatrix} \quad K_p=\begin{bmatrix} K_{pt} & 0 \\ 0 & K_{ps} \end{bmatrix} \quad K_i=\begin{bmatrix} K_{it} & 0 \\ 0 & K_{is} \end{bmatrix}$$
$$K_d=\begin{bmatrix} K_{dt} & 0 \\ 0 & K_{ds} \end{bmatrix} \qquad e=\begin{bmatrix} e_t \\ e_s \end{bmatrix}=\begin{bmatrix} \theta_{1\mathrm{d}}-\theta_1 \\ \theta_{2\mathrm{d}}-\theta_2 \end{bmatrix} \tag{22}$$

where i_t and i_s are the input current into the valves of thigh and shank as seen in Eq. (19), respectively. k_{pt}, k_{it} and k_{dt} are the fixed proportional, integral and differential gains for the robotic thigh, respectively. k_{ps}, k_{is} and k_{ds} are the fixed proportional, integral and differential gains for the robotic shank, respectively.

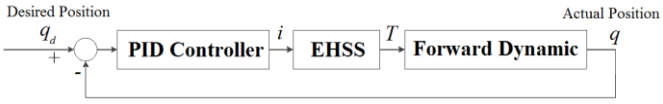

Fig. 2. The block diagram of the PID controller scheme

B. Design of the Velocity Feedback Control

For the conventional PID controller, the angular velocities are obtained using the electrical integration method as shown in Eq. (5). In this paper, we take use of an observer to estimate the angular velocities. The observer can be written as

$$\begin{cases} \hat{v}=z_v+k_v q \\ \dot{z}_v=-k_v\hat{v} \end{cases} \tag{23}$$

where

$$\hat{v}=\begin{bmatrix} \hat{v}_t \\ \hat{v}_s \end{bmatrix} \quad z_v=\begin{bmatrix} z_{vt} \\ z_{vs} \end{bmatrix} \quad k_v=\begin{bmatrix} k_{vt} & 0 \\ 0 & k_{vs} \end{bmatrix} \quad q=\begin{bmatrix} \theta_1 \\ \theta_2 \end{bmatrix} \tag{24}$$

where z_{vt} and z_{vs} are the observer states; k_{vt} and k_{vs} are the observer gains to ensure convergence of the error to zero; $\hat{v}_t$ and $\hat{v}_s$ are the estimated angular velocity of the thigh and shank.

The estimated velocity can be used in the feedback loop of the position controller to decrease the tracking error. The proposed controller is obtained through adding a velocity error term to a proportional controller, which is shown in the block diagram of Fig. 3. The control law can be expressed as

$$i(t)=\alpha(q_d-q)+\beta(v_d-\hat{v}) \tag{25}$$

where

$$q_d=\begin{bmatrix} \theta_{1\mathrm{d}} \\ \theta_{2\mathrm{d}} \end{bmatrix} \quad q=\begin{bmatrix} \theta_1 \\ \theta_2 \end{bmatrix} \quad v_d=\begin{bmatrix} \dot{\theta}_{1d} \\ \dot{\theta}_{2d} \end{bmatrix} \quad \hat{v}=\begin{bmatrix} \hat{v}_t \\ \hat{v}_s \end{bmatrix}$$
$$\alpha=\begin{bmatrix} \alpha_t & 0 \\ 0 & \alpha_s \end{bmatrix} \quad \beta=\begin{bmatrix} \beta_t & 0 \\ 0 & \beta_s \end{bmatrix} \tag{26}$$

where α_t, β_t, α_s and β_s are fixed controller gains. In fact, this controller is a state feedback controller where the velocity term represents the internal state of the actuation system.

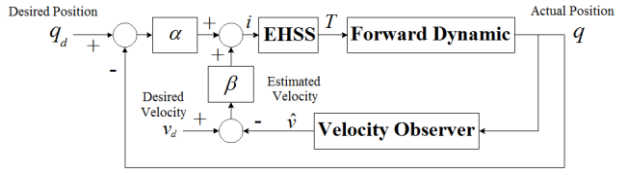

Fig. 3. The block diagram of the velocity feedback controller scheme

IV. Simulation Results

A. Selection of System Parameters

In order to demonstrate the effectiveness of this system, the EHSS and the 2-DOF robotic legs are simulated with the following nominal parameters: m_t=7kg, m_s=3.26kg, L_t=0.43m, L_s=0.5m, L_{Gt}=0.24m, L_{Gs}=0.28m, I_t=0.13$kg{\cdot}m^2$, I_s=0.07$kg{\cdot}m^2$, A_{p1}=1.77×10$^{-4}m^2$, a=0.14m, b=0.26m, c=0.17m, d=0.28m, P_s=2×10^6Pa, P_r=0.5×10^5Pa, L_0=0.1m, x_{p0}=0.08m, β=2×10^7Pa, V_0=1.15×10$^{-4}m^3$, C_t=8×10$^{-12}m^5N^{-1}s^{-1}$, g_s=3.97×10^{-8}m^{4}s^{-1}N$^{-1/2}$.

B. Selection of Observer Gains

To establish conditions on the gains k_v to ensure the observer stability, we consider the error between the actual velocity v and its estimate $\hat{v}$.

$$e_v=v-\hat{v} \tag{27}$$

Differentiating both sides of the above equation yields an analytic expression that describes the rate of change of the error e_v. From the Eq. (24), the differential equation of the error e_v is expressed as

$$\dot{e}_v=-\dot{z}_v-k_v\dot{v}=k_v\hat{v}-k_v\dot{v}=k_v(\hat{v}-\dot{v}) \tag{28}$$

To make the observer stable to be used in the EHSS and 2-DOF robotic legs, the Lyapunov function should be satisfied that

$$V=e_v\dot{e}_v=(v-\hat{v})k_v(\hat{v}-v)=-k_v(\hat{v}-v)^2<0 \tag{29}$$

The selection of observer gain must be obeyed that k_v>0. After massive trials, the optimum of observer gains is made that k_{vt}=30 and k_{vs}=520.

C. Selection of Controller Gains

The gains of the conventional PID controller are chosen using Ziegler-Nichols method. Then, optimum gains of k_{pt}=60, k_{it}=40 and k_{dt}=150 are obtained for the controller to track the position of the robotic thigh. In addition, the gains for the controller to take the best position tracking of the robotic shank are selected that k_{ps}=120, k_{is}=40 and k_{ds}=130. The optimal values for the gains of the velocity feedback controller are made that α_t=260, β_t=65, α_s=120 and β_s=160.

D. Comparison Results Between the PID Controller and Velocity Feedback Controller

The system simulation can be implemented by Matlab based on the introduced EHSS model and mathematical 2-DOF robotic leg model. The computer simulations are conducted using two types of controllers, such as PID controller and velocity feed back controller.

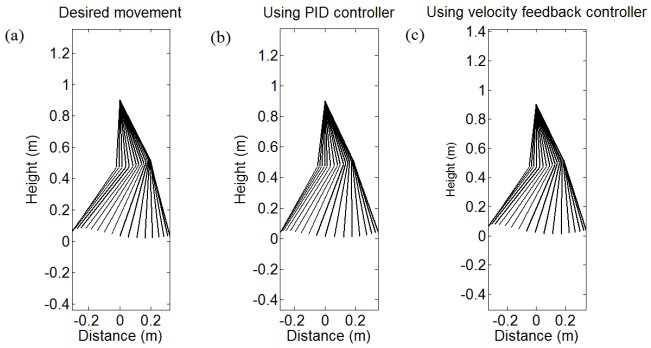

Fig. 4. Tracking performance for robotic leg: (a) Desired movements for robotic leg, (b) Actual movements using PID controller, (c) Actual movements using velocity feedback controller

The desired movements for 2-DOF robotic leg are demonstrated in Fig. 4(a), while Fig. 4(b) and Fig. 4(c) give the actual movement using the PID controller and velocity feedback controller, respectively. However, the control effects for both controllers can not be considered as comparable results. In order to display the controller effect comparatively, the controller performances are indicated by the mean absolute error (MAE) and tracking lag.

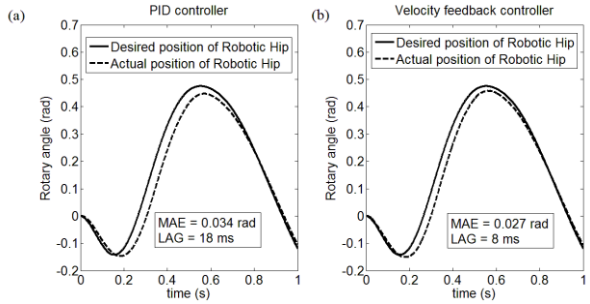

Fig. 5. Tracking performance for robotic hip using: (a) PID controller, (b) Velocity feedback controller

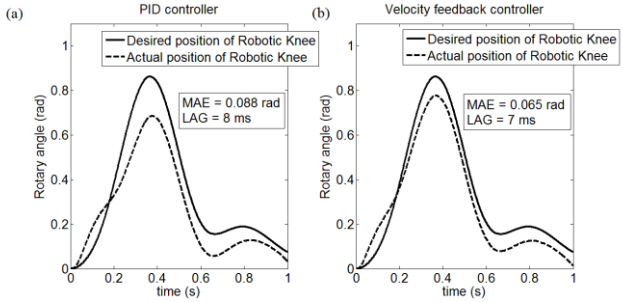

Fig. 6. Tracking performance for robotic knee using: (a) PID controller, (b) Velocity feedback controller

As Fig. 5 shows, the control performance for robotic hip using velocity feedback controller obtains less MAE (0.027 rad) and less tracking lag (8 ms) than that using PID controller (MAE=0.034 rad, and lag=18 ms). According to the MAE and lag values displayed in Fig. 6, using the velocity feedback controller (MAE=0.065 rad, and lag =7 ms) results in reduction of position error and tracking lag compared with the PID controller (MAE=0.088 rad, and lag =8 ms). The comparative results suggest that the velocity feedback controller gives better performance for 2-DOF robotic leg.

For velocity feedback controller, the velocity is estimated using an observer as seen in Eq. (23). However, the velocity is acquired using integral way for PID controller. As described in Fig. 7 and Fig. 8, the estimated velocity using observer is more smooth compared with that using integral way.

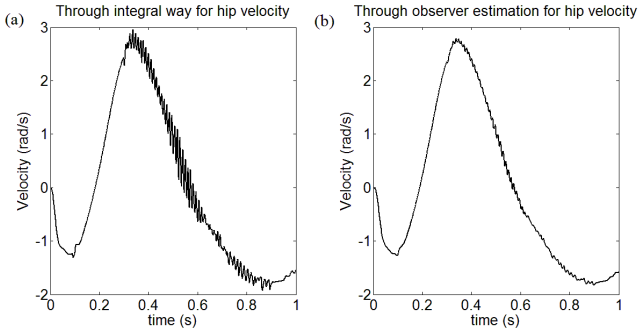

Fig. 7. The acquired velocity for robotic hip: (a) Through integral way, (b) Through observer estimation

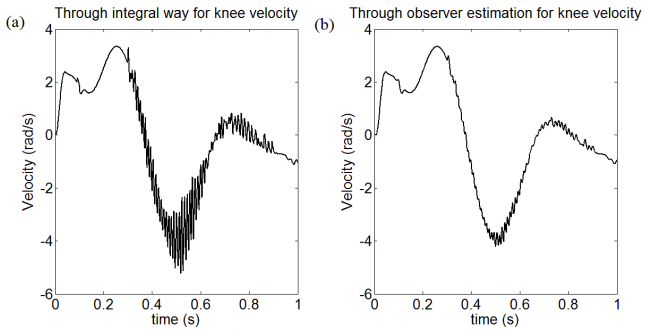

Fig. 8. The acquired velocity for robotic knee: (a) Through integral way, (b) Through observer estimation

V. Conclusion

A mathematical and computational model of 2-DOF robotic leg driven by EHSS has been successfully developed, simulated and tested in MATLAB software. The approach to mimic the lower thigh and shank segments of the human leg is original and unique to use the mathematical concepts and the Lagrange equation to achieve the system dynamic. In addition, the velocity feedback controller is proposed to track the position trajectory of 2-DOF robotic leg, while an observer is used to estimate the velocity. Two types of controllers, such as the conventional PID controller and the velocity feedback controller, are taken to obtain comparative results. Compared with the PID controller, the simulation results show that the proposed velocity feedback controller acquires less MAE and less tracking lag in term of position control strategy.

Acknowledgment

This research is supported and funded by Hubei Digital Manufacturing Key Laboratory and Key Laboratory of Fiber Optic Sensing Technology and Information Processing. We also thank the anonymous reviewers and editors for their valuable comments and suggestions.

References

[1] K. J. Meessen, J. J. H. Paulides, and E. A. Lomonova, "Analysis and design considerations of a 2-DOF rotary-linear actuator," *in Proc. IEEE Int. Elect. Mach. Drives Conf.*, pp. 336–341, 2011.

[2] P. Bolognesi, "A novel rotary-linear permanent magnets synchronous machine using common active parts," *in Proc. 15th IEEE Mediterranean Electrotech. Conf.*, pp. 1179–1183, 2010.

[3] J. K. Si, H. C. Feng, L. W. Ai, Y. H. Hu, "Design and Analysis of a 2-DOF Split-Stator Induction Motor," *IEEE Transaction on energy conversion*, vol. 30, no. 3, pp. 1200-1208, 2015.

[4] K. J. Meessen, J. J. H. Paulides, and E. A. Lomonova, “Analysis of a novel magnetization pattern for 2-DoF rotary-linear actuators,” *IEEE Trans. Magn*., vol. 48, no. 11, pp. 3867–3870, 2012.

[5] E. A. Mendrela and E. Gierczak, “Double-winding rotary-linear induction motor,” *IEEE Trans. Energy Convers*., vol. EC-2, no. 1, pp. 47–54, 1987.

[6] J. Fleszar and E. A. Mendrela, “Twin-armature rotary-linear induction motor,” *IEEE Proc. B*, vol. 130, no. 3, pp. 186–192, 1983.

[7] J. C. Gao and P. D. Wu, “A fuzzy neural network controller in the electrohydraulic position control system,” *IEEE international conference on intelligent systems*, (1997), October 28-31; Beijing, China.

[8] C. L. Hwang, “Neural-Network-Based Variable Structure Control of Electrohydraulic Servosystems Subject to huge uncertainties without persistent excitation,” *IEEE/ASME Transactions on mechatronics*, vol. 4, no. 1, pp. 50-59, 1999.

[9] F. Srairi, L. Saidi, F. Djeffal, and M. Meguellati, "Modeling, Control and Optimization of a New Swimming Microrobot Design," *Engineering Letters*, vol. 24, no.1, pp. 106-112, 2016.

[10] E. Deticek, “An intelligent position control of electrohydraulic drive using hybrid fuzzy control structure”, *Proceedings of the IEEE International Symposium on Industrial Electronics*., vol.3, pp. 1008-1013, 1999.

[11] T. L. Chern and Y. C. Wu, “An optimal variable structure control with integral compensation for electrohydraulic position servo control systems”, *IEEE transaction on industrial electronics*., vol. 39, no. 5, pp. 460-463, 1992.

[12] Q. P. Ha, Q. Nguyen, D. C. Rye and H. F. Durrant-Whyte, “Sliding mode control with fuzzy tuning for eletrohydraulic position servo system”, *1998 second international conference on knowledge-based intelligent electronic system*, April, 1998.

[13] G. Hasanifard, M. H. Zarif and A. A. Ghareveisi, “Nonlinear robust backstepping control of an electrohydraulic velocity servo system”, *Mediterranean conference on control and automation*, July, 2007

[14] S. Tafazoli, C. W. de Silva and P. D. Lawrence, “Tracking control of an elechydraulic manipulator in the presence of friction”, *IEEE Transactions on control system technology*, May, 1998.

[15] S. Tafazoli, C. W. de Silva and P. D. Lawrence, “Friction estimation in a planar electrohydraulic manipulator”, *Proceedings of the American control conferences, Seatle, American*, June. pp. 401-411, 1995.

[16] Zhongda Tian, Shujiang Li, Yanhong Wang, and Quan Zhang, "Multi Permanent Magnet Synchronous Motor Synchronization Control based on Variable Universe Fuzzy PI Method," *Engineering Letters*, vol. 23, no.3, pp. 180-188, 2015.

[17] J. Y. Yao, Z. X. Jiao and S. S. Han, “Friction compensation for low velocity control of hydraulic flight motion simulator: A simple adaptive robust approach”, *Chinese Journal of Aeronautics*., vol. 26, no. 3, pp. 814-822, 2013.

[18] J. Y. Yao, Z. X. Jiao and B. YAO, “Robust Control for Static Loading of Electro-hydraulic Load Simulator with Friction Compensation”, *Chinese Journal of Aeronautics*., vol. 25, no. 6, pp. 954-962, 2012.

[19] T. A. Adam, H. R. Abdul, Y. L. Cheng, “Adaptive controller algorithm for 2-DOF humanoid robot arm,” *2nd International Conference on System-Integrated Intelligence: Challenges for Product and Production Engineering, Procedia Technology*, pp. 765-774, 2014.